Inorganic Chemistry

pubs.acs.org/IC

Article

Modulation of Isomerization and Ligand Exchange Rates by π Bonding in Bis(iminoxolene)iridium Pyridine Complexes

Thomas H. Do, David A. Haungs, William Y. Chin, Jack T. Jerit, Analena VanderZwaag, and Seth N. Brown*

Cite This: *Inorg. Chem.* 2023, 62, 11718–11730

Read Online

ACCESS | Metrics & More | Article Recommendations | Supporting Information

ABSTRACT: The bis(iminoxolene)iridium complex $(Diso)_2IrCl$ (Diso = *N*-(2,6-diisopropylphenyl)-4,6-di-*tert*-butyl-2-imino-*o*-benzoquinone) reacts with pyridine to give *trans*-$(Diso)_2Ir(py)Cl$ as the kinetic product, with *cis*-$(Diso)_2Ir(py)Cl$ formed as the exclusive thermodynamic product upon heating. Electronic spectra and density functional theory calculations point to very similar electronic structures for the cis and trans isomers, with a nonbonding iminoxolene-centered HOMO and a metal−iminoxolene π* LUMO. The triplet states of *cis*-$(Diso)_2Ir(py)Cl$ and *cis*-$[(Diso)_2Ir(py)_2]^+$ (but not *trans*-$(Diso)_2Ir(py)Cl$) are unusually low in energy (1000−1500 cm^{-1} above the singlets), as shown by variable-temperature NMR spectroscopy. The low-energy triplets are attributed to a change in dihedral angle in the iminoxolenes, which allows a partial π interaction that cannot be achieved in the trans octahedral compounds. Mechanistic studies of the trans−cis isomerization in toluene indicate that the reaction proceeds via isomerization of the five-coordinate species to a form with cis iminoxolene ligands and an apical oxygen. This form is high in energy due to the loss of a secondary iminoxolene-to-iridium π-donor interaction that is possible in the trans form but not in the cis form for the square pyramidal structures. This stereoelectronic effect, combined with the poorer binding of pyridine in *trans*-$(Diso)_2Ir(py)Cl$ due to the interactions of the *N*-aryl substituents with the pyridine, makes the pyridine dissociate faster from the trans isomer by a factor of 10^8 at room temperature.

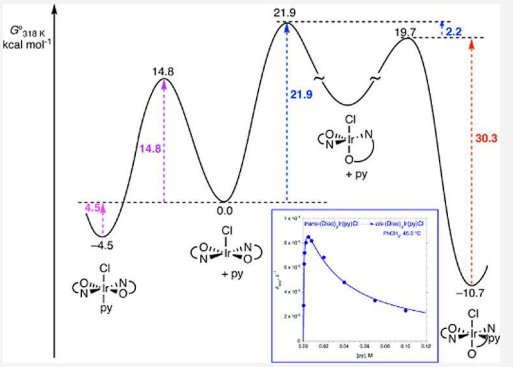

INTRODUCTION

Substitution reactions are ubiquitous in chemistry and play an integral role in many multistep reactions. One important general observation about dissociative substitution reactions is that they can be significantly accelerated by π-donating groups bonded to the atom from which the group is dissociating. A classic example of this in organic chemistry involves carbonyl chemistry, where the rapid breakdown of the tetrahedral intermediate is driven by the formation of a carbon−oxygen π bond (Figure 1a). A classic example of this in inorganic chemistry involves the basic hydrolysis of cobalt(III) am(m)ine halides,[1] where rapid substitution reactions result from the deprotonation of an am(m)ine ligand and its π donation to cobalt in the five-coordinate intermediate (Figure 1b).[2] In each case, rate acceleration results from the possibility of π bonding in the lower-coordinate intermediate (and, at least to some extent, in the transition state) that is unavailable in the reactant.

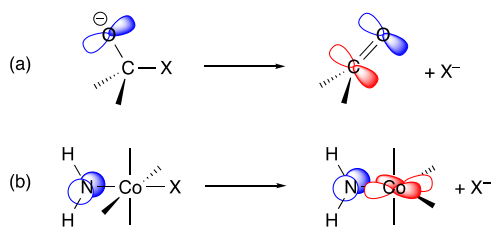

Figure 1. Examples of π-accelerated dissociative substitution reactions in (a) organic carbonyl chemistry and (b) inorganic ligand exchange.

Donors of π electrons may be groups as well as single atoms. One such potentially π-donating group is the 2-amidophenoxide ligand (Figure 2). This redox-active ligand is able to adopt overall formal oxidation states ranging from −2 (amidophenoxide) to −1 (iminosemiquinone) to 0 (iminoquinone); in order to be able to refer to it without regard to formal oxidation state, it is conveniently designated an iminoxolene ligand by analogy to the familiar dioxolene and dithiolene ligands.[3] The key ligand π orbital—the HOMO of the amidophenoxide, the SOMO of the iminosemiquinone, and the LUMO of the iminoquinone—can be referred to as the redox-active orbital or RAO, without reference to the overall oxidation state. This

Received: May 25, 2023
Published: July 12, 2023

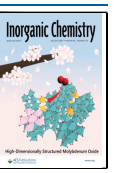

https://doi.org/10.1021/acs.inorgchem.3c01717
Inorg. Chem. 2023, 62, 11718−11730

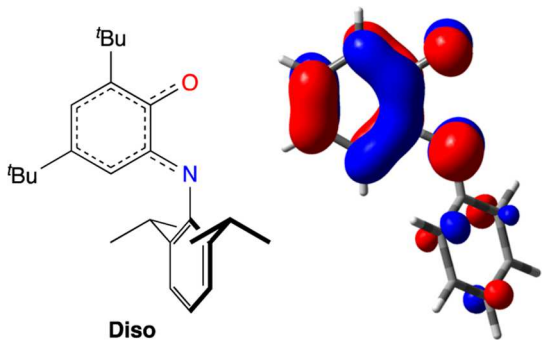

Figure 2. Iminoxolene ligand Diso and Kohn–Sham RAO of iminoxolene ligand ap (o-C_6H_4(NPh)O).

orbital has significant density on both the nitrogen and oxygen atoms, though more on the nitrogen, and is of moderate energy similar to that of metal d orbitals of elements in the middle of the transition series. This leads to strong and highly covalent interactions in molybdenum tris(iminoxolenes)[4] and in ruthenium and osmium bis- and tris(iminoxolene) complexes.[5]

Recently, we prepared the five-coordinate iridium bis(iminoxolene) complex $(Diso)_2IrCl$ (Diso = *N*-(2,6-diisopropylphenyl)-4,6-di-*tert*-butyl-2-imino-*o*-benzoquinone), which adopts a square pyramidal geometry with apical chloride.[6] The major metal–iminoxolene π interaction involves the *B*-symmetry combination of RAOs. However, the *A*-symmetry combination of RAOs, which would be nonbonding if the $(Diso)_2Ir$ fragment were strictly planar, can donate to the empty Ir d_{z^2} orbital due to the pyramidalization at iridium (Figure 3).

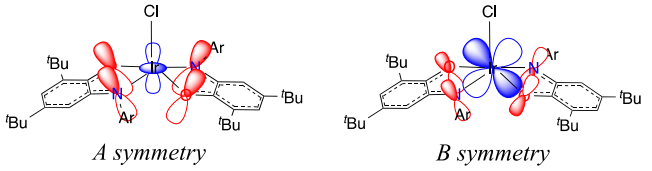

Figure 3. Schematic depiction of metal–iminoxolene π-bonding interactions in $(Diso)_2IrCl$. Only contributions from iridium, nitrogen, and oxygen are shown.

This secondary π interaction was observed to have noticeable effects on the optical spectrum of $(Diso)_2IrCl$. The qualitative effects of this π interaction on ligand substitution were discussed in a recent study of a mixed iminoxolene-dioxolene complex $(\kappa^2,\eta^2$-Tipsi)(3,5-^{t}Bu$_2$Cat)IrCl (Tipsi = *N*-(2,6-bis(triisopropylsilylethynyl)phenyl)-4,6-di-*tert*-butyl-2-imino-*o*-benzoquinone).[7] In this complex, displacement of the bound alkyne by pyridine results in stereoisomerization from cis to trans. This was explained by the intermediacy of a five-coordinate structure where the stability of the isomer with apical chloride, which uniquely enables iminoxolene π donation to the d_{z^2}, funnels all other five-coordinate stereoisomers into the trans geometry.

Here, we report the addition reactions of pyridine to $(Diso)_2IrCl$ to form six-coordinate adducts. *trans*-$(Diso)_2Ir(py)Cl$ is the kinetic product of this addition, but upon heating, the thermodynamic cis isomer (or, under some conditions, cationic *cis*-$[(Diso)_2Ir(py)_2]Cl$) is formed. The cis (but not the trans) compounds show NMR spectra with significant temperature-dependent chemical shifts characteristic of compounds with low-lying triplet states. This highlights stereochemical differences in π bonding that are not readily apparent in the structures or optical spectra of the compounds. Kinetic studies strongly support the intermediacy of a five-coordinate cis isomer in the isomerization reaction. This intermediate is high in energy because of the unavailability of the π interaction that is possible in the trans isomer, and this engenders a marked acceleration of pyridine dissociation in the trans isomer.

RESULTS AND DISCUSSION

Synthesis of Bis(iminoxolene)iridium Pyridine Complexes. The square pyramidal bis(iminoxolene)iridium complex $(Diso)_2IrCl$ reacts rapidly with pyridine at room temperature to form *trans*-$(Diso)_2Ir(py)Cl$ (eq 1). The binding of

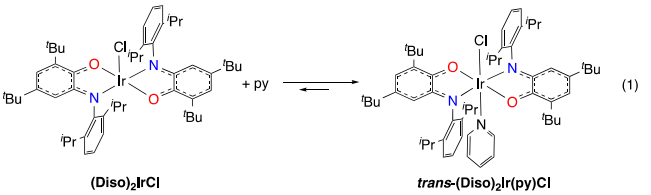

pyridine is favorable but not overwhelmingly so: dissolution of crystalline *trans*-$(Diso)_2Ir(py)Cl$ at room temperature results in solutions whose NMR spectra show predominantly the trans adduct, but small amounts of free pyridine and five-coordinate $(Diso)_2IrCl$ are also observable (Figure S20). Resonances for all three species are sharp, indicating that ligand dissociation is slow on the NMR timescale. This allows one to assess the symmetry of the adduct as C_2, consistent with the trans stereoisomer. Dissolution of crystalline *trans*-$(Diso)_2Ir(py)Cl$ in toluene-d_8 and subsequent measurement of the concentrations of $(Diso)_2IrCl$, *trans*-$(Diso)_2Ir(py)Cl$, and free pyridine at equilibrium allows one to determine a value of K_1 = 8900 at 297 K, with measurements from 297 to 328 K giving ΔH°_1 = −17.8(6) kcal mol^{-1} and ΔS°_1 = −41.9(18) cal mol^{-1} K^{-1} (Figure S21).

When *trans*-$(Diso)_2Ir(py)Cl$, formed from the reaction of $(Diso)_2IrCl$ with pyridine, is heated in the presence of low concentrations of pyridine, it isomerizes to *cis*-$(Diso)_2Ir(py)Cl$ (eq 2), with the appearance of a new set of NMR resonances

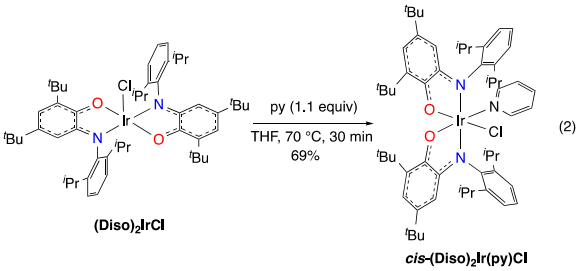

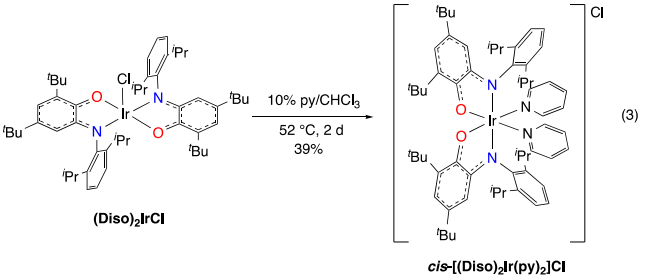

attributable to a C_1-symmetric complex. The isomerization is quantitative and irreversible, with no trans isomer observable at

https://doi.org/10.1021/acs.inorgchem.3c01717
Inorg. Chem. 2023, 62, 11718–11730

Table 1. Summary of Crystal Data

	trans-$(Diso)_2IrCl(py)$	*cis*-$(Diso)_2IrCl(py)\cdot CHCl_3$	*cis*-$(Diso)_2IrCl(py)\cdot PhCH_3$	*cis*-$[(Diso)_2Ir(py)_2]Cl\cdot 4CHCl_3\cdot C_5H_{12}$
molecular formula	$C_{57}H_{79}ClIrN_3O_2$	$C_{58}H_{80}Cl_4IrN_3O_2$	$C_{64}H_{87}ClIrN_3O_2$	$C_{71}H_{100}Cl_{13}IrN_4O_2$
formula mass	1065.88	1185.25	1158.01	1694.68
T (K)			120(2)	
crystal system	monoclinic	monoclinic	monoclinic	orthorhombic
space group	$P2_1/c$	$C2/c$	$P2_1/c$	$Fddd$
λ (Å)			0.71073 (Mo Kα)	
total data	242 982	190 488	131 301	284 443
indep refls	26 464	13 926	12 846	9653
R_{int}	0.0561	0.0530	0.0469	0.0491
obsd refls [$I > 2\sigma(I)$]	22 305	11 928	11 534	8343
a (Å)	25.528(4)	40.142(5)	21.715(3)	26.928(2)
b (Å)	19.015(3)	17.2414(19)	17.179(4)	27.385(2)
c (Å)	24.669(4)	16.2440(18)	16.177(4)	42.315(4)
α (°)	90	90	90	90
β (°)	116.899(2)	91.9899(17)	105.085(7)	90
γ (°)	90	90	90	90
V (Å^3)	10 679(3)	11 236(2)	5827(2)	31 204(4)
Z	8	8	4	16
μ (mm^{-1})	2.593	2.610	2.382	2.202
crystal size (mm)	0.26 × 0.15 × 0.10	0.15 × 0.13 × 0.13	0.18 × 0.17 × 0.12	0.16 × 0.14 × 0.13
refined params	1785	933	988	565
$R1$, $wR2$ [$I > \sigma(I)$]	0.0268, 0.0489	0.0212, 0.0399	0.0224, 0.0427	0.0293, 0.0709
$R1$, $wR2$ [all data]	0.0395, 0.0522	0.0304, 0.0422	0.0278, 0.0441	0.0379, 0.0762
goodness of fit	1.060	1.021	1.074	1.057

long reaction times. If the trans isomer is heated in chloroform at high concentrations of pyridine, then a C_2-symmetric, cationic bis(pyridine) adduct *cis*-$[(Diso)_2Ir(py)_2]Cl$ is isolated in modest yields (eq 3). The cationic bis(pyridine) complex is not observed if *cis*-$(Diso)_2Ir(py)Cl$ is prepared and subsequently heated with excess pyridine.

The structures of the three pyridine adducts have been determined in the solid state (Table 1 and Figure 4). In the two cis compounds, the nitrogen atoms of the iminoxolene ligands are mutually trans, as expected on steric grounds and as has been observed in *cis*-$(Diso)_2IrCl_2$.[6] The metal−iminoxolene distances (Table 2) are unexceptional, and the iridium-pyridine distances are similar to those that have been observed previously in octahedral compounds where pyridine is trans to halide[7,8] or to oxygen.[9] The C−C, C−O, and C−N distances in the iminoxolenes can be used to calculate a metrical oxidation state (MOS),[10] which reflects the ligand-centered electron density in the iminoxolene frontier π orbital (the RAO) and hence can be used to gauge the extent to which the filled metal−iminoxolene π orbitals are ligand- or metal-centered. The observed MOS values in the trans pyridine adduct (−1.29(2)) and of the iminoxolene trans to Cl in the cis pyridine adduct (−1.26(6)) are indistinguishable from the MOS value displayed by five-coordinate $(Diso)_2IrCl$ (−1.27(7)). The values for the iminoxolene ligands trans to pyridine in *cis*-$(Diso)_2Ir(py)Cl$ (−1.18(4)) or in *cis*-$[(Diso)_2Ir(py)_2]^+$ (−1.14(8)) are slightly more positive. This difference is also observed in the structure of *cis*-$(ap)_2Ir(py)Cl$ calculated by DFT (ap = 1,2-C_6H_4(NPh)O; MOS values = −1.16(7) trans to pyridine and −1.39(7) trans to Cl).

Electronic Structure of Bis(iminoxolene)iridium Pyridine Adducts. The pyridine adduct *trans*-$(Diso)_2Ir(py)Cl$ is isoelectronic with the osmium complexes *trans*-$(^{H}ap)_2Os(PR_3)_2$[11] or *trans*-$(Clip)Os(py)_2$ ($ClipH_4$ = 2,2′-biphenylbis(3,5-di-*tert*-butyl-2-hydroxyphenylamine)),[5] while *cis*-$(Diso)_2Ir(py)Cl$ is isoelectronic with group 8 compounds such as *cis*-$(^{H}ap)_2Os(P[OR]_3)_2$[11] or $Os(L_{N,O,S})_2$ ($H_2L_{N,O,S}$ = *N*-(2-methylthiophenyl)-3,5-di-*tert*-butyl-2-hydroxyaniline).[12] DFT calculations on $(ap)_2Ir(py)Cl$ support electronic structures that are analogous to these examples (Figure 5). In the trans isomer, the *B*-symmetry combination of the iminoxolene RAOs interacts very strongly with an iridium dπ orbital. The LUMO of the molecule is the π^* combination of these orbitals. In contrast, the *A*-symmetry RAO combination is essentially nonbonding with respect to the iridium (in the group 8 compounds, it is A_u and thus strictly nonbonding). The six-coordinate adduct thus differs significantly from the five-coordinate $(ap)_2IrCl$, where pyramidalization at iridium allows the *A*-symmetry RAO combination (which is the compound's HOMO) to donate to the Ir-d_{z^2} orbital, which is Ir−Cl σ^* in character.

This difference in bonding is manifested in the optical spectrum of *trans*-$(Diso)_2Ir(py)Cl$ (Figure 6). Five-coordinate $(Diso)_2IrCl$ shows two prominent bands of similar intensity ($\varepsilon \sim 10^4$ L mol^{-1} cm^{-1}) in the visible region: a HOMO−LUMO transition at 710 nm and a higher-energy band at 478 nm assigned to a transition from the *B*-symmetry metal−iminoxolene π-bonding orbital to the antibonding combination between the Ir−Cl σ^* orbital and the *A*-symmetry RAO.[6] In contrast, the optical spectrum of *trans*-$(Diso)_2Ir(py)Cl$ is dominated by the HOMO−LUMO transition, which is at a lower energy (λ_{max} = 909 nm) and has a higher intensity ($\varepsilon = 3 \times 10^4$ L mol^{-1} cm^{-1}) than the corresponding transition in the five-coordinate species. The $\pi(B) \rightarrow \sigma^*(A)$ transition is not apparent as it is expected to shift to higher energy (since the *A*-symmetry virtual orbital is σ^* to both Cl and pyridine) and lower intensity (since the virtual orbital has little iminoxolene character).

In the cis geometry, the two ligand RAO orbitals transform as $A + B$ (in idealized C_2 symmetry, as in *cis*-$(Diso)_2Ir(py)_2^+$), and both find symmetry matches in the metal dπ orbitals. One would

https://doi.org/10.1021/acs.inorgchem.3c01717
Inorg. Chem. 2023, 62, 11718−11730

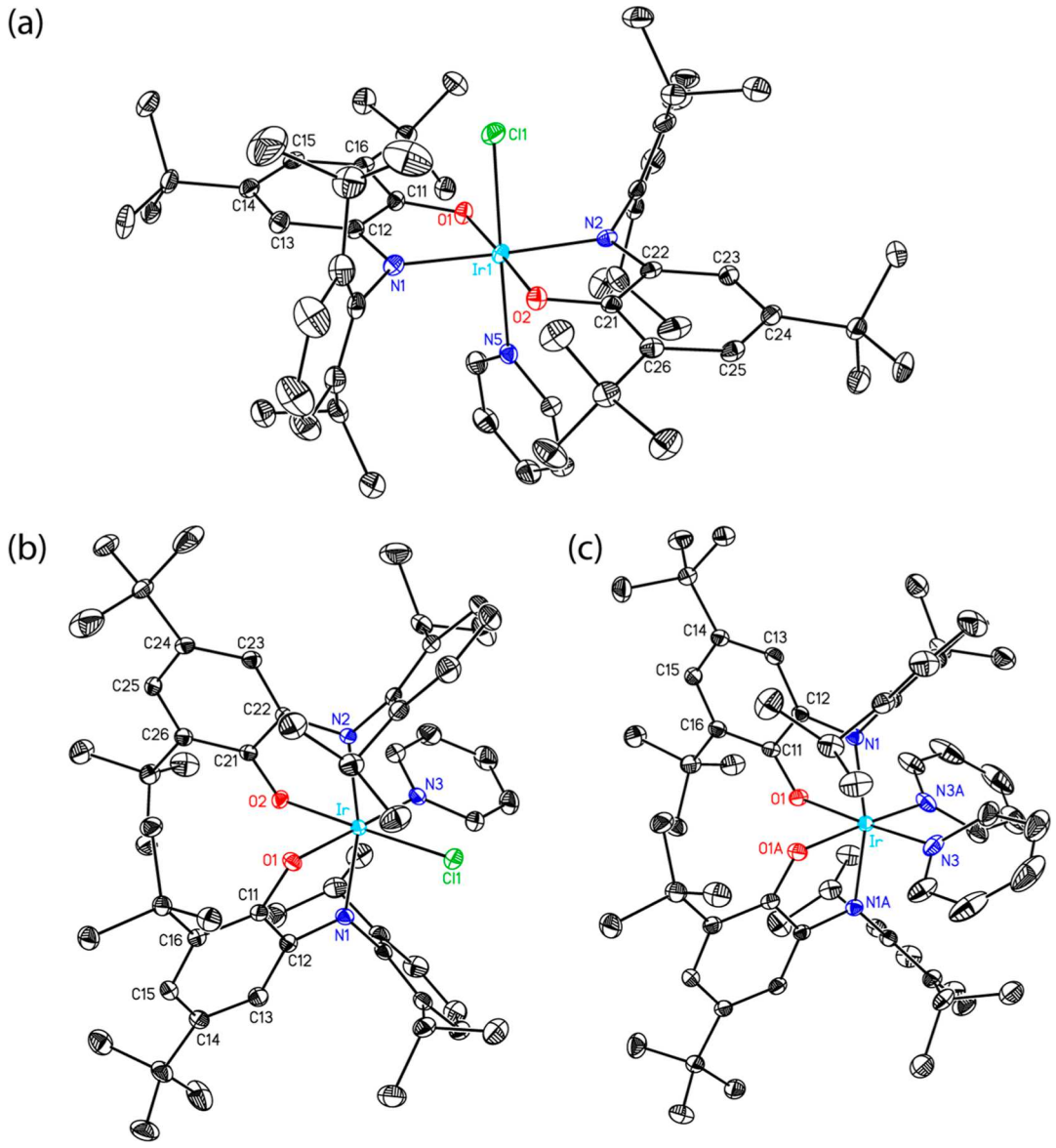

Figure 4. Thermal ellipsoid plots of (a) *trans*-$(Diso)_2Ir(py)Cl$, (b) *cis*-$(Diso)_2Ir(py)Cl{\cdot}CHCl_3$, and (c) *cis*-$[(Diso)_2Ir(py)_2]Cl{\cdot}4CHCl_3{\cdot}C_5H_{12}$. Hydrogen atoms, counterions, and lattice solvent are omitted for clarity. Only one of the two crystallographically inequivalent molecules of *trans*-$(Diso)_2Ir(py)Cl$ is shown.

thus expect the four π orbitals to combine to form two π bonding and two π^* orbitals; six electrons would fill two bonding and one antibonding orbital. In fact, the iminoxolene ligands of cis compounds with this electron configuration are observed to fold significantly away from the monodentate ligands, decreasing the π overlap between the *B*-symmetry ligand combination and metal dπ orbitals.[11] In *cis*-$(Diso)_2Ir(py)Cl$, the X−Ir−O1−C11 dihedral angles average 112.0(6)° in the two crystal structures, and the dihedral angle is 105.3° in the solid-state structure of *cis*-$[(Diso)_2Ir(py)_2]^+$. Computationally, the dihedral angles average 110.4° in *cis*-$(ap)_2Ir(py)Cl$ and 109.8° in $[(ap)_2Ir(py)_2]^+$. A calculated structure for *cis*-$(ap)_2Ir(py)Cl$ with acute dihedral angles (74.5° avg.) could be found as a local minimum, but it is calculated to be 5.9 kcal mol^{-1} higher in free energy than the minimum-energy structure.

Differences in the electronic structures of the cis and trans isomers manifest in their NMR spectra. *trans*-$(Diso)_2Ir(py)Cl$ shows normal chemical shifts in its ^1H NMR spectrum, with the iminoxolene ring protons resonating between 6.0 and 6.5 ppm (Figure 7a). In contrast, the two cis compounds show notably upfield shifts for the iminoxolene ring hydrogens, which appear between 3.5 and 5 ppm in *cis*-$(Diso)_2Ir(py)Cl$ (Figure 7b) and at δ −2.6 and −16.0 ppm in *cis*-$[(Diso)_2Ir(py)_2]Cl$ (Figure 7c). Other signals are also shifted from their normal positions in the two cis compounds, though less dramatically than the iminoxolene peaks.

Discrepant chemical shifts have been observed in other iminoxolene compounds in cases where the compounds have a low-lying, thermally populated triplet state.[13,14] This origin of the large chemical shifts causes a characteristic nonlinear deviation of the chemical shifts away from their diamagnetic values as temperature increases due to the exponential growth of the triplet population. This contrasts with the $1/T$-dependence of chemical shifts in simple Curie paramagnets, which causes signals to move toward the diamagnetic region as temperature increases. The chemical shifts of the two cis compounds show

https://doi.org/10.1021/acs.inorgchem.3c01717
Inorg. Chem. 2023, 62, 11718−11730

Table 2. Selected Distances (Å) and MOS Values Derived from Crystal Structures of Bis(iminoxolene)iridium Pyridine Compounds[a]

	trans-$(Diso)_2Ir(py)Cl$	*cis*-$(Diso)_2Ir(py)Cl$		*cis*-$[(Diso)_2Ir(py)_2]^+$
		ring trans to py	ring trans to Cl	
Ir−O1	2.011(9)	2.004(3)	2.000(3)	2.0056(17)
Ir−N1	2.008(13)	2.014(4)	2.026(5)	2.034(2)
Ir−N3	2.101(3)	2.081(4)		2.072(2)
Ir−Cl	2.332(4)	2.350(4)		
O1−C11	1.322(5)	1.320(3)	1.328(2)	1.323(3)
N1−C12	1.364(8)	1.360(7)	1.365(3)	1.357(3)
C11−C12	1.426(4)	1.431(4)	1.434(3)	1.433(3)
C12−C13	1.410(4)	1.418(3)	1.418(9)	1.426(3)
C13−C14	1.375(4)	1.371(3)	1.376(5)	1.365(4)
C14−C15	1.417(5)	1.424(3)	1.424(5)	1.427(4)
C15−C16	1.387(4)	1.381(3)	1.383(3)	1.379(4)
C16−C11	1.420(4)	1.424(5)	1.419(4)	1.421(4)
MOS[10]	−1.29(2)	−1.18(5)	−1.26(6)	−1.14(8)

[a]For the chloro compounds, metrical data are averaged among chemically equivalent values (for *trans*-$(Diso)_2Ir(py)Cl$, among the two compounds in the asymmetric unit; for *cis*-$(Diso)_2Ir(py)Cl$, between the chloroform and the toluene solvates). The stated esd's reflect both the variance in the measured values and the statistical uncertainty of the crystallographic model.

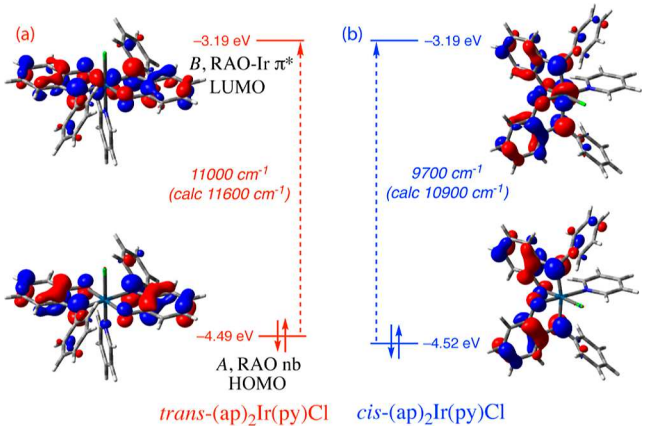

Figure 5. Frontier MO diagrams of (a) *trans*-$(ap)_2Ir(py)Cl$ and (b) *cis*-$(ap)_2Ir(py)Cl$.

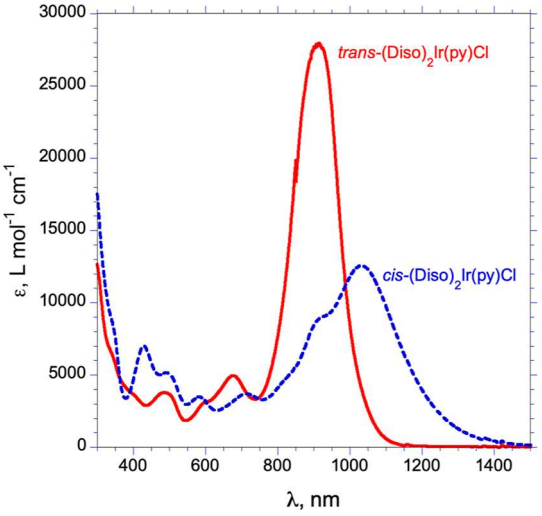

Figure 6. Optical spectra in CH_2Cl_2 of *trans*-$(Diso)_2Ir(py)Cl$ (in 5.7 mM pyridine, red solid line) and *cis*-$(Diso)_2Ir(py)Cl$ (blue dashed line).

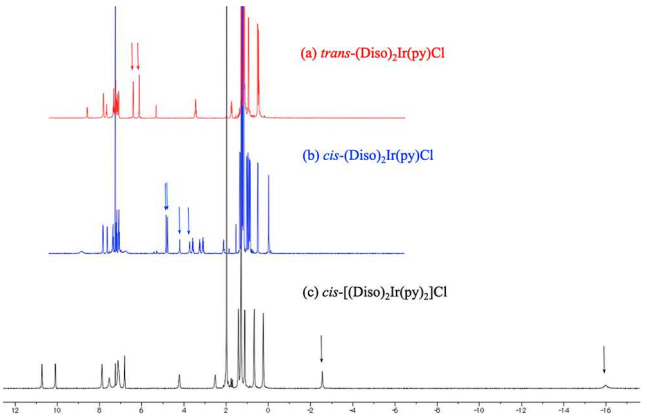

Figure 7. ^1H NMR spectra ($CDCl_3$, 23 °C) for (a) *trans*-$(Diso)_2Ir(py)Cl$, (b) *cis*-$(Diso)_2Ir(py)Cl$, and (c) *cis*-$[(Diso)_2Ir(py)_2]Cl$. Iminoxolene hydrogens are indicated with arrows.

the expected nonlinear dependence for a singlet−triplet equilibrium (Figures 8 and S15−S19). Analysis of the temperature dependence allows one to calculate the singlet−triplet gaps in these compounds,[15] as well as the hyperfine couplings, which show good correlations with the values calculated by DFT (Table S1). The larger shifts in *cis*-$[(Diso)_2Ir(py)_2]^+$ are principally due to its smaller singlet−triplet gap (1053(7) cm^{-1} vs 1473(10) cm^{-1} for *cis*-$(Diso)_2Ir(py)Cl$).

The triplet states of the cis compounds have both nominally antibonding orbitals singly occupied, so both the *A*- and the *B*-symmetry combinations have a net π-bond order of 0.5. It is thus energetically favorable for the dihedral angle of the iminoxolene ligands to relax because a smaller dihedral angle increases the net π interaction among the *B* orbitals. DFT calculations on the triplet states of *cis*-$(ap)_2Ir(py)Cl$ and *cis*-$[(ap)_2Ir(py)_2]^+$ give dihedral angles of 92.0° (avg.) and 96.9°, respectively. This allows the triplet to be lower in energy in the cis compounds than in the trans where there is no analogous distortion that can improve π bonding. In effect, the triplet state geometry allows the latent antibonding character of the HOMO of the cis

https://doi.org/10.1021/acs.inorgchem.3c01717
Inorg. Chem. 2023, 62, 11718−11730

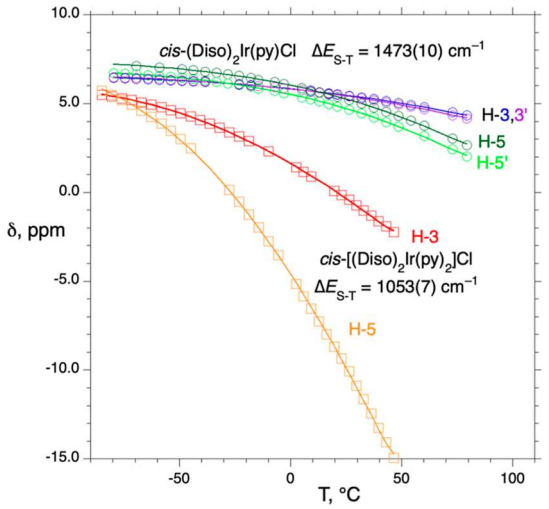

Figure 8. Temperature-dependent chemical shifts of iminoxolene protons in *cis*-$(Diso)_2Ir(py)Cl$ (toluene-d_8, circles) and *cis*-$[(Diso)_2Ir(py)_2]Cl$ (acetone-d_6, squares). Solid lines are the best fits to eq 6.

compounds to become patent, so these compounds act as if the HOMO and LUMO are both π^* and relatively close in energy.

Kinetics of Ligand Substitution Reactions of *cis*- and *trans*-$(Diso)_2Ir(py)Cl$. While the exchange of free pyridine with bound pyridine in *trans*-$(Diso)_2Ir(py)Cl$ is slow on the NMR timescale, equilibration between the pyridine adduct and five-coordinate $(Diso)_2IrCl$ is complete in less than a minute at ambient temperatures and above. The addition of pyridine to $(Diso)_2IrCl$ to give *trans*-$(Diso)_2Ir(py)Cl$ (eq 1, forward direction) can be observed by optical spectroscopy at sub-ambient temperatures (Figure 9). The transformation proceeds smoothly without detectable intermediates, as indicated by the presence of tight isosbestic points. At these temperatures and concentrations of pyridine, the binding equilibrium lies very far to the right, so the reverse reaction can be neglected. Reactions are first order in iridium in the presence of excess pyridine, and k_{obs} values are linearly dependent on pyridine concentration

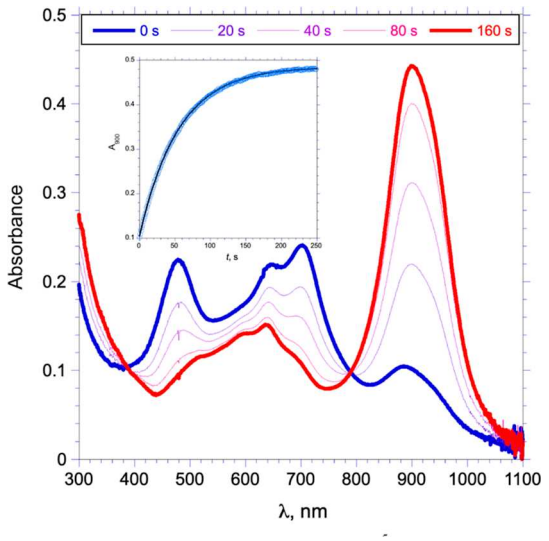

Figure 9. Successive optical spectra of $(Diso)_2IrCl$ (1.6×10^{-5} M) treated with pyridine (3.9×10^{-4} M) in toluene at 0.0 °C. Inset: A_{900} as a function of time, with the solid line being the best fit to first-order kinetics.

(Figure S22), indicating an overall second-order addition reaction. At 10 °C, the second-order rate constant k_1 is 92(5) L mol^{-1} s^{-1}, and Eyring analysis of the temperature dependence of the rate constant between −40 and 10 °C (Figure 10a) gives

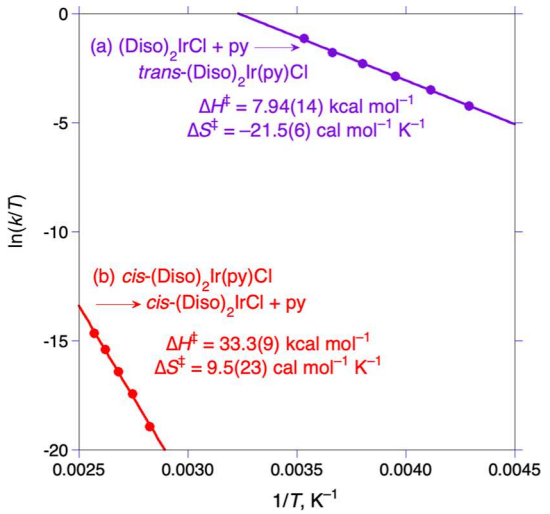

Figure 10. Eyring plots of $\ln(k/T)$ as a function of $1/T$ for (a) the addition of pyridine to $(Diso)_2IrCl$ to give *trans*-$(Diso)_2Ir(py)Cl$ (purple circles) and (b) for the exchange of py with py-d_5 in *cis*-$(Diso)_2Ir(py)Cl$ (red circles). Both reactions were studied in toluene.

$\Delta H^{\ddagger} = 7.94(14)$ kcal mol^{-1} and $\Delta S^{\ddagger} = -21.5(6)$ cal mol^{-1} K^{-1}. When combined with the thermodynamics of the binding equilibrium measured by NMR (eq 1), one can determine the activation parameters for pyridine dissociation from *trans*-$(Diso)_2Ir(py)Cl$ as $\Delta H^{\ddagger} = 25.7(6)$ kcal mol^{-1} and $\Delta S^{\ddagger} = 20.4(19)$ cal mol^{-1} K^{-1}. This corresponds to a dissociation rate constant k_{-1} of 0.025 s^{-1} ($t_{1/2} = 27$ s) at 298 K. The rather facile dissociation of pyridine from the bis(iminoxolene) complex contrasts with the ~5×10^4 times slower dissociation from the analogous mono-iminoxolene mono-dioxolene complexes *trans*-(Tipsi)(3,5-^{t}Bu$_2$Cat)Ir(py)Cl (Tipsi = *N*-(2,6-bis-(triisopropylsilylethynyl)phenyl)-4,6-di-*tert*-butyl-2-imino-*o*-benzoquinone), which exchange with deuterated pyridine with rate constants of about 6×10^{-5} s^{-1} (depending on the orientation of the catecholate) at 60 °C.[7] The arylimino group makes the iminoxolene a much stronger donor than the dioxolene, and the metal is correspondingly less Lewis acidic. This trend has been observed previously in replacing catecholates with amidophenoxides in molybdenum bis- and tris-catecholate complexes.[16,17]

Pyridine exchange in *cis*-$(Diso)_2Ir(py)Cl$ is much slower than in the trans isomer. Treatment of *cis*-$(Diso)_2Ir(py)Cl$ with pyridine-d_5 at room temperature does not result in deuterium incorporation into the complex at any appreciable rate. To observe significant exchange (eq 4), heating to temperatures

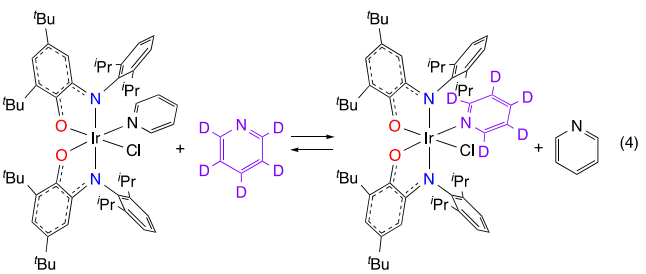

https://doi.org/10.1021/acs.inorgchem.3c01717
Inorg. Chem. 2023, 62, 11718−11730

above 80 °C is required (Figure S24). The observed first-order rate constants[18] for the release of free pyridine-h_5 are found to be independent of the concentration of added pyridine-d_5, consistent with a dissociative exchange mechanism. Eyring analysis in the range of 81−116 °C (Figure 10b) gives activation parameters $\Delta H^{\ddagger}$ = 33.3(9) kcal mol^{-1} and $\Delta S^{\ddagger}$ = 9.5(23) cal mol^{-1} K^{-1}. Extrapolation to room temperature gives k_4 (298 K) = 3×10^{-10} s^{-1}. Dissociation of pyridine at room temperature is thus 10^8 times faster from the trans isomer than from the cis isomer of (Diso)$_2$Ir(py)Cl.

Kinetics and Mechanism of trans to cis Isomerization of (Diso)$_2$Ir(py)Cl. The trans isomer of (Diso)$_2$Ir(py)Cl isomerizes quantitatively to the cis isomer over the course of hours at 45 °C. At these temperatures, dissociation of pyridine from the trans isomer is quite fast (extrapolated k_{-1} = 0.4 s^{-1}), so *trans*-(Diso)$_2$Ir(py)Cl is effectively always in equilibrium with five-coordinate (Diso)$_2$IrCl, with the relative populations of the two compounds determined by the pyridine concentration. This can be observed by UV−visible spectroscopy, where at low concentrations, initial spectra show prominent bands at 705 nm and 480 nm due to the five-coordinate complex, while the strong 900 nm band of six-coordinate *trans*-(Diso)$_2$Ir(py)Cl predominates in initial spectra at higher concentrations of pyridine (Figure 11). In either case, the *trans*-(Diso)$_2$Ir(py)Cl/(Diso)$_2$IrCl mixture transforms smoothly over time to give exclusively *cis*-(Diso)$_2$Ir(py)Cl. Kinetic measurements carried out with excess pyridine always conform to first-order decay, allowing the determination of k_{obs} as a function of pyridine concentration (Table S5).

The observed first-order rate constants for isomerization show an unusual, non-monotonic dependence on pyridine concentration (Figure 12). Qualitatively, at low pyridine concentrations, where substantial amounts of the five-coordinate complex are present, the isomerization is accelerated by increasing pyridine. At high pyridine concentrations, where almost all the reactant is found as six-coordinate *trans*-(Diso)$_2$Ir(py)Cl, the reaction is inhibited by pyridine. This pattern, particularly the pyridine inhibition at high [py], has clear mechanistic implications. It requires that isomerization involves pyridine dissociation from *trans*-(Diso)$_2$Ir(py)Cl so that the concentration of the active intermediate is inversely proportional to [py] (under conditions where almost all the reactant is in the form of *trans*-(Diso)$_2$Ir(py)Cl). Furthermore, it requires that the rate-determining step (at least at high [py]) must be unimolecular in the five-coordinate species and must *not* involve pyridine, as a reaction of pyridine with the intermediate would be first order in pyridine, which would cancel out the pyridine inhibition of the formation of the intermediate and give an overall order of zero in pyridine.

These mechanistic requirements strongly suggest that isomerization proceeds through reversible dissociation of pyridine to give (Diso)$_2$IrCl which then undergoes unimolecular isomerization (Scheme 1). Presumably, this isomerization would give a cis five-coordinate structure in which one of the iminoxolene oxygens is apical in the square pyramid. DFT calculations find such a structure for (ap)$_2$IrCl as a local minimum, with a free energy 11.9 kcal mol^{-1} higher than the structure with apical chlorine. Pyridine binding to the open site in the square pyramid would then afford the *cis*-(Diso)$_2$Ir(py)Cl product. Application of the steady-state approximation to the unobserved five-coordinate *cis*-(Diso)$_2$IrCl, with (Diso)$_2$IrCl + py/*trans*-(Diso)$_2$Ir(py)Cl treated as a rapid (though not necessarily favorable) equilibrium, gives eq 5 as the expected rate law (derivation given in the Supporting Information). This expression gives an excellent fit to the observed data (Figure 12),

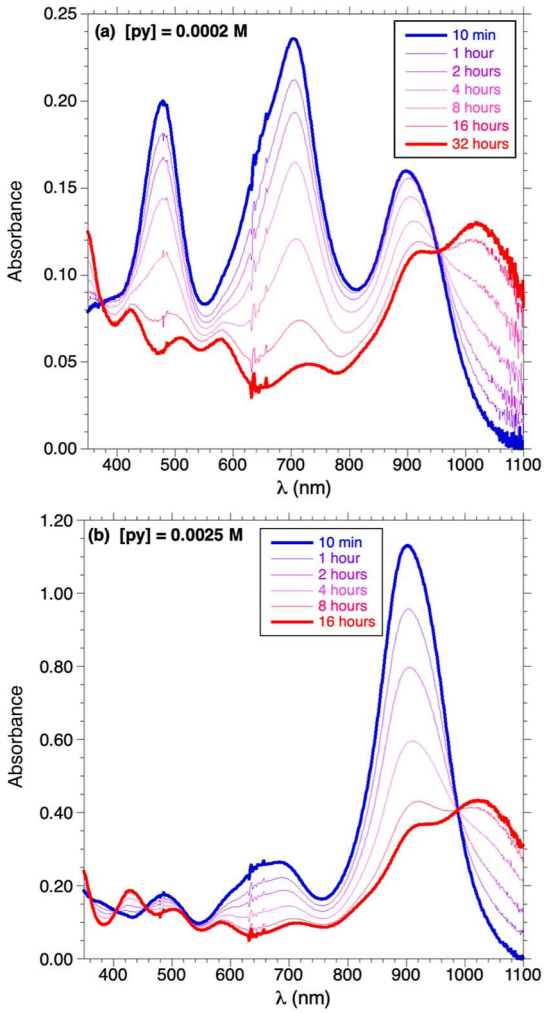

Figure 11. Time dependence of the optical spectra of mixtures of (Diso)$_2$IrCl and pyridine in toluene at 45.0 °C at (a) [py] = 2.0×10^{-4} M ([Ir] = 1.0×10^{-5} M) and (b) [py] = 2.5×10^{-3} M ([Ir] = 3.5×10^{-5} M).

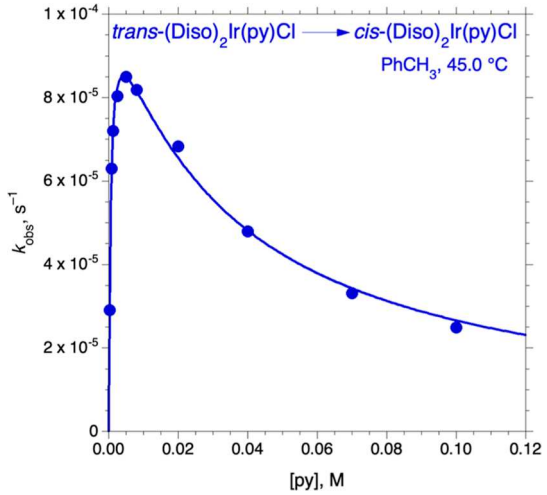

Figure 12. Variation of k_{obs} for the formation of *cis*-(Diso)$_2$Ir(py)Cl with pyridine concentration. The solid line represents the best fit to eq 5.

https://doi.org/10.1021/acs.inorgchem.3c01717
Inorg. Chem. 2023, 62, 11718−11730

Scheme 1. Proposed Mechanism for trans to cis Isomerization of $(Diso)_2Ir(py)Cl$

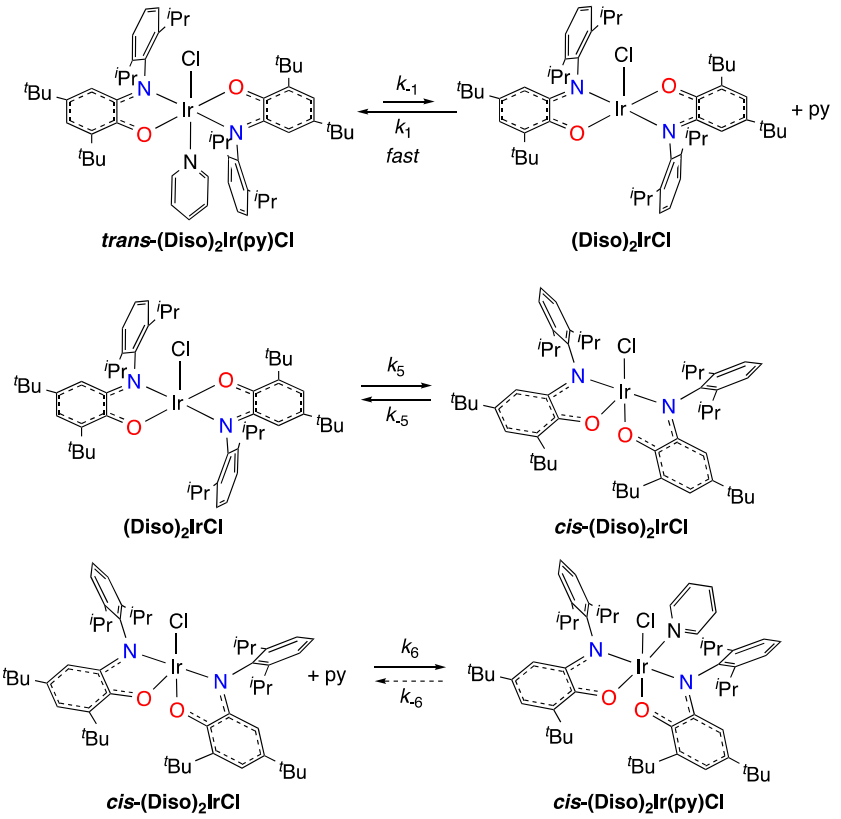

with the two kinetic parameters determined to be $k_5 = 0.0063(6)$ s^{-1} and $k_{-5}/k_6 = 0.0326(19)$ M. The value of K_1 of 1800 determined from the fit is in reasonable agreement with the value of 1200 determined at 45 °C by NMR.

$$k_{obs} = \frac{k_5[py]}{(\{k_{-5}/k_6\} + [py])(1 + K_1[py])} \quad (5)$$

Summary and Interpretation of the Energy Landscape for Substitution and Isomerization. Using the thermodynamics of pyridine binding in *trans*-$(Diso)_2Ir(py)Cl$ (K_1), the kinetics of binding of pyridine to $(Diso)_2IrCl$ to give *trans*-$(Diso)_2Ir(py)Cl$ (k_{-1}), the kinetics of dissociation of pyridine from *cis*-$(Diso)_2Ir(py)Cl$ (k_4), and the kinetics of trans to cis isomerization (k_5, k_{-5}/k_6), one can place nearly all the relevant species and transition states of the $(Diso)_2IrCl$/py system on a common free energy scale at 318 K (Figure 13). The only species whose free energy is not well determined is the unobserved five-coordinate complex *cis*-$(Diso)_2IrCl$. Computationally, using the stripped-down ap ligand (ap = 1,2-$C_6H_4(O)(NPh)$), the cis structure is observed to be 11.9 kcal mol^{-1} above $(ap)_2IrCl$ (Figure 14). Inclusion of the 2,6-diisopropyl substituents barely changes this figure (to 10.3 kcal mol^{-1}).

Three key points emerge from this free energy landscape: (1) *cis-(Diso)$_2$Ir(py)Cl is modestly more stable than trans-(Diso)$_2$Ir(py)Cl.* The trans to cis isomerization is favorable, with $\Delta G^\circ_{trans\rightarrow cis} = -6.1$ kcal mol^{-1} and $K_{trans\rightarrow cis} = 1.6 \times 10^4$ at 318 K. The preference of the octahedral compounds for the cis isomer is likely due to the steric profile of the 2,6-diisopropylphenyl groups in Diso. Thus, computationally, $(ap)_2Ir(py)Cl$ actually prefers the trans isomer (by 5.1 kcal mol^{-1}), while $(diso)_2Ir(py)Cl$ prefers the cis isomer by 5.7 kcal

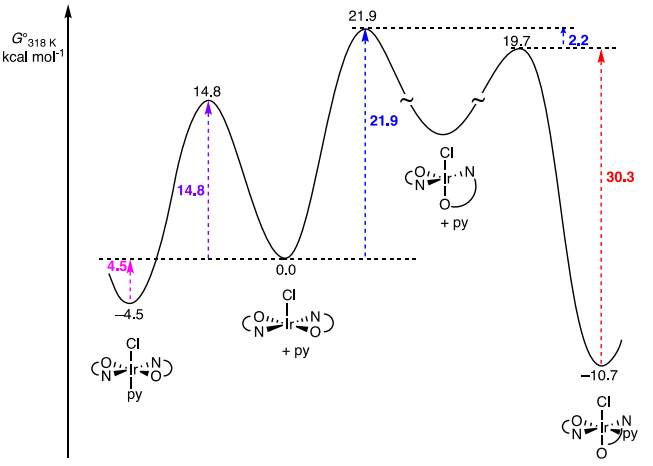

Figure 13. Experimental reaction coordinate for $(Diso)_2IrCl$ + pyridine. All values are standard free energies for the reactions in toluene at 318 K in kcal mol^{-1}. Boldface values next to dashed arrows are directly measured, from equilibration of $(Diso)_2IrCl$ and py with *trans*-$(Diso)_2Ir(py)Cl$ (pink); kinetics of binding of pyridine to $(Diso)_2IrCl$ (purple); kinetics of isomerization to form *cis*-$(Diso)_2Ir(py)Cl$ from $(Diso)_2IrCl$ and pyridine (blue); and kinetics of py/py-d_5 exchange in *cis*-$(Diso)_2Ir(py)Cl$ (red). Values in black represent standard free energies relative to $(Diso)_2IrCl$ + py.

mol^{-1}, in good agreement with the experimental result (diso = 1,2-$C_6H_4(O)$(N-2,6-$^i Pr_2C_6H_3$); Figure 14). (Note that while the calculations on $(diso)_2Ir(py)Cl$ accurately reproduce the relative binding of pyridine to the cis and trans isomers, they underestimate the absolute binding strength of pyridine by about 18 kcal mol^{-1}. The qualitative underestimation of pyridine binding has been observed previously in calculations on mixed

https://doi.org/10.1021/acs.inorgchem.3c01717
Inorg. Chem. 2023, 62, 11718−11730

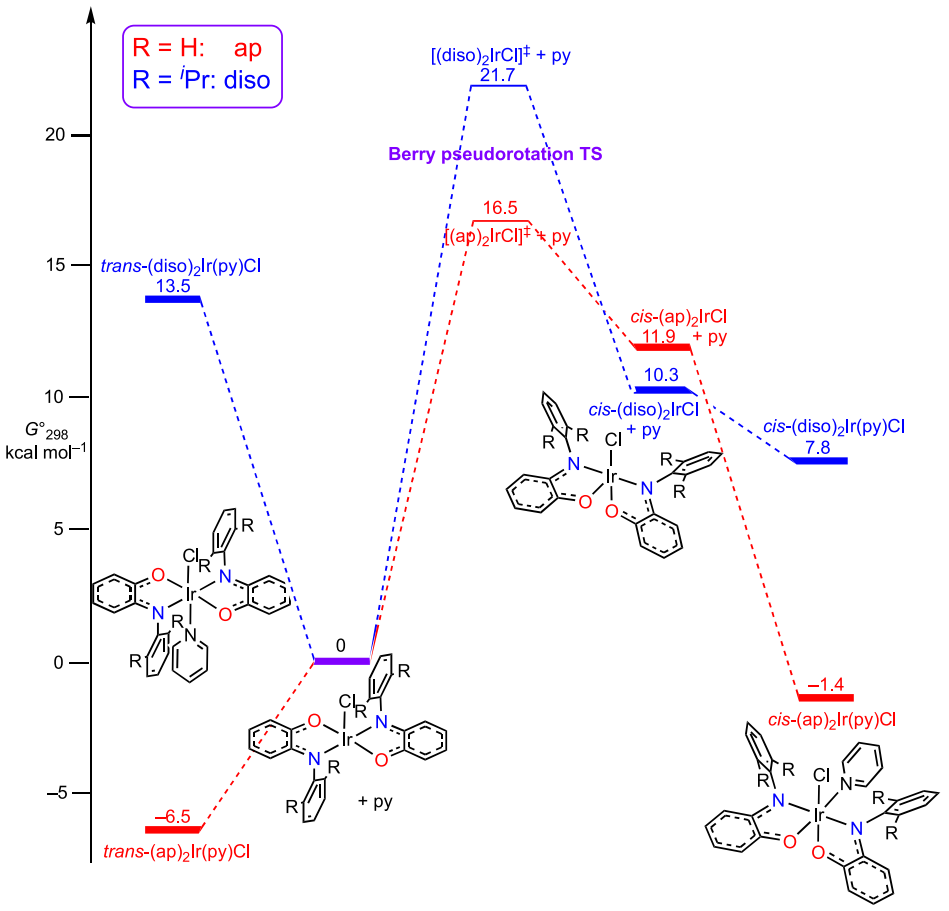

Figure 14. Calculated free energies of $(L)_2IrCl$ + pyridine (B3LYP, gas phase, SDD basis set for Ir, 6-31G* basis set for other atoms). L = ap shown in red and L = diso shown in blue. Standard free energies are given at 298 K in kcal mol^{-1} relative to $(L)_2IrCl$/free pyridine at 0 kcal mol^{-1}.

iminoxolene-dioxolene iridium systems.[7]) The conformation of the Diso ligand, with the plane of the *N*-aryl group perpendicular to the iminoxolene plane, orients the isopropyl groups so that they interact strongly with the ligands that are cis to both N and O of Diso. In *trans*-$(Diso)_2Ir(py)Cl$, there are two such interactions with the bound pyridine, while in *cis*-$(Diso)_2Ir(py)Cl$, there is only one. Any electronic preference for the trans isomer is apparently modest and easily overcome by this steric effect. This is consistent with the analysis of the bonding and spectra of the two isomers, which point to a very similar electronic structure with a ligand-centered nonbonding HOMO and a single strong metal−ligand π interaction (Figure 5). The cis isomer has the potential to have an antibonding interaction between the filled ligand-centered orbital and a filled dπ orbital. This is realized in the triplet state, lowering the singlet−triplet energy gap, whereas in the singlet state, this antibonding interaction is largely avoided by folding of the iminoxolene ligands.

(2) *Five-coordinate* trans-*$(Diso)_2IrCl$ is much more stable than* cis-*$(Diso)_2IrCl$.* Dissociation of a ligand from octahedral $(Diso)_2Ir(py)Cl$ has the result of substantially lowering the energy of one of the d orbitals (d_{z^2} in the square pyramid, with *z* taken along the Ir-axial ligand bond), opening the possibility of turning on a stabilizing interaction between this orbital and the RAO-centered HOMO. This possibility is realized in the trans geometry, where there is a good overlap with the *A*-symmetry RAO combination (Figure 15a), but not in the cis geometry, where the overlap is poor (Figure 15b). As a result, isolated

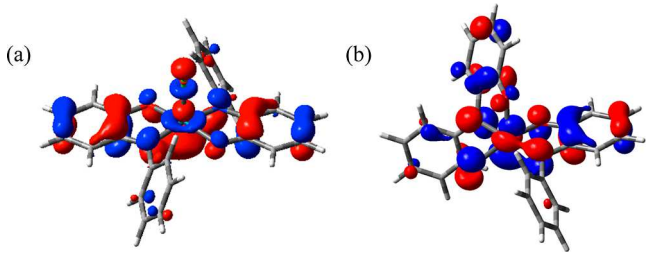

Figure 15. Kohn−Sham HOMO of (a) $(ap)_2IrCl$[6] and (b) *cis*-$(ap)_2IrCl$.

$(Diso)_2IrCl$ is a square pyramid with apical chloride and trans iminoxolenes.[6] The cis isomer with apical oxygen is computed to be a local minimum with a much higher free energy that is relatively insensitive to sterics (calculated ΔG° = 11.9 kcal mol^{-1} for $(ap)_2IrCl$ and 10.3 kcal mol^{-1} for $(diso)_2IrCl$, Figure 14). The experimental data on the trans to cis isomerization strongly support the intermediacy of a high-energy five-coordinate structure. The non-monotonic dependence of the rate on pyridine concentration indicates that the isomerization takes place in a unimolecular reaction of a five-coordinate species. The isomeric five-coordinate species must then be trapped by added pyridine to conform to the observed rate law. Given the observed structure of *cis*-$(Diso)_2Ir(py)Cl$ (cis-α with pyridine trans to oxygen), this strongly suggests that the intermediate has a square pyramidal structure with apical oxygen. Its high energy

https://doi.org/10.1021/acs.inorgchem.3c01717
Inorg. Chem. 2023, 62, 11718−11730

is suggested by the high barrier to its formation from $(Diso)_2IrCl$ ($\Delta G^{\ddagger}$ = 21.9 kcal mol^{-1} at 45 °C).

The greater stability of the five-coordinate species with apical chloride was also invoked in the ligand substitution chemistry of the mixed iminoxolene-dioxolene complex (η^2,κ^2-Tipsi)-(3,5-^{t}BuCat)IrCl (Tipsi = *N*-(2,6-bis(triisopropylsilylethynyl)-phenyl)-4,6-di-*tert*-butyl-2-imino-*o*-benzoquinone).[7] In the iminoxolene-dioxolene complex, however, the experimental observation is the exclusive formation of *trans*-(κ^2-Tipsi)(3,5-^{t}BuCat)Ir(py)Cl on the addition of pyridine to the cis complex of the internal alkyne. This is proposed to take place via initial formation of a variety of stereoisomers of five-coordinate (κ^2-Tipsi)(3,5-^{t}BuCat)IrCl, which all funnel down in energy to the more stable *trans*-(κ^2-Tipsi)(3,5-^{t}BuCat)IrCl before trapping by pyridine can take place. This contrasts with the reactions of $(Diso)_2IrCl$, where the addition of pyridine to *cis*-$(Diso)_2IrCl$ is competitive with the re-formation of *trans*-$(Diso)_2IrCl$ (k_6/k_{-5} = 31 M^{-1} at 45 °C). The low rate of dissociation of pyridine from *trans*-(κ^2-Tipsi)(3,5-^{t}BuCat)Ir-(py)Cl strongly suggests that this product is formed under kinetic control (dissociation of pyridine from a cis six-coordinate complex would likely be even slower, vide infra). It thus appears that *cis*-$(Diso)_2IrCl$ undergoes pyridine addition significantly faster, or isomerizes to *trans*-$(Diso)_2IrCl$ significantly slower, than its mono-dioxolene analogue. DFT calculations strongly support the latter notion, with the more hindered *cis*-$(diso)_2IrCl$ computed to have an isomerization barrier of 11.4 kcal mol^{-1}, much higher than the barrier for *cis*-$(ap)_2IrCl$ of 4.6 kcal mol^{-1} (Figure 14). The latter value is in line with the calculated barriers of 1.3 to 8.7 kcal mol^{-1} for stereoisomerization of the various isomers of *cis*-(Tipsi)(cat)IrCl,[7] which are also relatively unhindered around the metal center.

(3) *Pyridine is much more labile in* trans-*$(Diso)_2Ir(py)Cl$ than in* cis-*$(Diso)_2Ir(py)Cl$.* Qualitatively, pyridine binding to give *trans*-$(Diso)_2Ir(py)Cl$ achieves equilibrium in minutes at room temperature, while the exchange of bound and free pyridine in *cis*-$(Diso)_2Ir(py)Cl$ takes weeks at 80 °C. Quantitatively, extrapolation of both dissociation rate constants to 45 °C indicates that dissociation of pyridine from the trans isomer has a barrier that is 11.0 kcal mol^{-1} lower than from the cis isomer, corresponding to rates that differ by a factor of 4×10^7. Some of this difference comes from the thermodynamic stabilization of the cis isomer by 6.1 kcal mol^{-1} relative to the trans isomer, an effect likely due to steric differences. The remaining 4.9 kcal mol^{-1} is due to kinetic factors: the transition state for pyridine addition to *cis*-$(Diso)_2IrCl$ is that much higher than the transition state for addition to *trans*-$(Diso)_2IrCl$, presumably largely because of the stabilization of the five-coordinate trans isomer due to the π-bonding effects discussed above.

The stereochemical effect on ligand lability is conceptually very similar to the stereoelectronic effects seen in base-catalyzed solvolyses of cobalt(III) polyamine complexes.[1,2] In these compounds, deprotonation of an amine generates a strongly π-donating amido ligand, which can accelerate the dissociation of a ligand if the pπ orbital on nitrogen is oriented properly to overlap with the newly low-lying empty $d_{x^2-y^2}$ orbital in the trigonal bipyramidal intermediate. For example, in (ethylenediaminediacetato)dichlorocobaltate(III) complexes, the *cis*-β isomer is 3×10^4 times more reactive than the *cis*-α isomer ($\Delta\Delta G^{\ddagger}$ = 6.1 kcal mol^{-1}).[19] Although the overall effect in $(Diso)_2Ir(py)Cl$ is noticeably larger than this, the portion of it due to π effects appears to be quite similar. Like the accessibility of amido π donation in cobalt(III) complexes, the possibility of iminoxolene-to-iridium π donation can have a noteworthy effect on rates of ligand substitution.

CONCLUSIONS

The five-coordinate complex $(Diso)_2IrCl$ reacts with pyridine to give *trans*-$(Diso)_2Ir(py)Cl$ as the kinetic product and *cis*-$(Diso)_2Ir(py)Cl$ as the thermodynamic product. The electronic structures of the six-coordinate compounds are very similar, with nonbonding iminoxolene-centered orbitals as the HOMO in each case. In the cis geometry, a metal−ligand antibonding interaction is avoided by the folding of the iminoxolene ligands. In the triplet state, this folding is smaller and the antibonding interaction is partially realized, which creates a small singlet−triplet gap in *cis*-$(Diso)_2Ir(py)Cl$ and *cis*-$[(Diso)_2Ir(py)_2]Cl$, giving rise to large temperature-dependent shifts in their ^{1}H NMR spectra.

The kinetics of trans to cis conversion, in particular a non-monotonic dependence of the rate on pyridine concentration, indicates a mechanism involving isomerization of $(Diso)_2IrCl$, which has a square pyramidal geometry with apical chloride, to a square pyramidal geometry with apical oxygen. This is relatively slow, principally because of the high energy of this isomer, whose geometry precludes π donation from the iminoxolene-centered HOMO to the iridium d_{z^2} orbital. Thermodynamically, the six-coordinate cis isomer is more stable than the trans isomer, mostly because it has fewer interactions between the bound pyridine and the isopropyl substituents on the iminoxolene ligand. The steric stabilization of *cis*-$(Diso)_2Ir(py)Cl$ and the electronic destabilization of the *cis*-$(Diso)_2IrCl$ intermediate formed on pyridine dissociation result in the trans isomer dissociating pyridine 10^8 times faster than the cis isomer at room temperature.

EXPERIMENTAL SECTION

General Procedures. Dried solvents were purchased from Acros Organics and stored in a nitrogen-filled drybox until use. Deuterated solvents were obtained from Cambridge Isotope Laboratories. $C_6D_5CD_3$ was dried over sodium, and CD_2Cl_2 was dried over 4A molecular sieves, followed by CaH_2. Deuterated solvents were vacuum transferred away from the drying agents and stored in the drybox prior to use. The iminoquinone Diso[20] and $(Diso)_2IrCl$[6] were prepared as described in the literature. NMR spectra were measured on a Bruker Avance DPX 400 MHz or 500 MHz spectrometer. Chemical shifts for ^{1}H and $^{13}C\{^1H\}$ spectra are reported in ppm downfield of TMS, with spectra referenced using the known chemical shifts of the solvent residuals. Infrared spectra were recorded by ATR on a Jasco 6300 FT-IR spectrometer and are reported in wavenumbers. Optical spectra were recorded in 1 cm quartz cells on an Agilent 8453 diode array spectrophotometer. Cyclic voltammograms were performed at a scan rate of 60 mV s^{-1} using a Metrohm Autolab PGSTAT128N potentiostat, with glassy carbon working and counter electrodes and a silver/silver chloride pseudo-reference electrode. The electrodes were connected to the potentiostat through electrical conduits in the drybox wall. Samples were 1 mM in analyte dissolved in CH_2Cl_2 with 0.1 M Bu_4NPF_6 as the electrolyte. Potentials were referenced to ferrocene/ferrocenium at 0 V.[21] The reference potentials were established by spiking the test solution with a small amount of decamethylferrocene (E° = −0.565 V vs Cp_2Fe^+/Cp_2Fe).[22] Elemental analyses were performed by Robertson Microlit Laboratories (Ledgewood, NJ) or Midwest Microlab (Indianapolis, IN).

***trans*-(Diso)$_2$Ir(py)Cl.** In a 20 mL scintillation vial in the drybox, $(Diso)_2IrCl$ (53.9 mg, 0.055 mmol), pyridine (5.0 μL, 0.62 mmol), and 3 mL of $CHCl_3$ are combined. The solution is allowed to react for 10 min at room temperature, layered with methanol, and then placed in a −37 °C freezer. After three days, the precipitated solid is collected by suction filtration and washed with 2 × 5 mL of MeOH. The teal solid is

https://doi.org/10.1021/acs.inorgchem.3c01717
Inorg. Chem. 2023, 62, 11718−11730

dried in vacuo for 30 min, yielding 50.3 mg of *trans*-$(Diso)_2Ir(py)Cl$ (86%). ^1H NMR ($CDCl_3$, spiked with pyridine to suppress the formation of $(Diso)_2IrCl$): δ 7.82 (d, 5.5 Hz, 2H, py 2,6-H), 7.63 (t, 7.7 Hz, 1H, py 4-H), 7.32 (dd, 7.7, 1 Hz, 2H, NAr 3- or 5-H), 7.22 (t, 7.7 Hz, 2H, NAr 4-H), 7.14 (t, 7.1 Hz, 2H, py 3,5-H), 7.04 (dd, 7.7, 1 Hz, 2H, NAr 3- or 5-H), 6.34 (d, 1.4 Hz, 2H, iminoxolene 3- or 5-H), 6.12 (d, 1.4 Hz, 2H, iminoxolene 3- or 5-H), 3.49 (sept, 6.6 Hz, 2H, $CHMe_2$), 1.66 (sept, 6.6 Hz, 2H, $CHMe_2$), 1.26 (s, 18H, ^{t}Bu), 1.18 (d, 6.6 Hz, 6H, $CH(CH_3)Me$), 1.12 (s, 18H, ^{t}Bu), 0.93 (d, 6.6 Hz, 6H, $CH(CH_3)Me$), 0.51 (d, 6.6 Hz, 6H, $CH(CH_3)Me$), 0.43 (d, 6.6 Hz, 6H, $CH(CH_3)Me$). $^{13}C\{^1H\}$ NMR ($CDCl_3$, spiked with pyridine): δ 181.20 (*C*O), 158.47, 150.37, 149.40, 145.06, 143.23, 141.44, 137.58, 136.88, 127.17, 125.62, 125.36, 125.26, 122.39, 114.70, 35.24 ($C(CH_3)_3$), 34.45 ($C(CH_3)_3$), 31.43 ($C(CH_3)_3$), 29.68 ($C(CH_3)_3$), 29.03 ($CH(CH_3)_2$), 28.84 ($CH(CH_3)_2$), 26.77 ($CH(CH_3)Me$), 26.42 ($CH(CH_3)Me$), 25.99 ($CH(CH_3)Me$), 23.06 ($CH(CH_3)Me$). IR (cm^{-1}): 3074 (w), 3060 (w), 2961 (m), 2924 (w), 2904 (w), 2863 (m), 1742 (w), 1712 (w), 1604 (w), 1590 (w), 1534 (m), 1521 (m), 1463 (m), 1446 (m), 1435 (m), 1392 (w), 1383 (m), 1357 (s), 1311 (s), 1279 (m), 1243 (s), 1232 (s), 1199 (s), 1160 (s), 1112 (m), 1067 (w), 1051 (m), 1023 (s), 999 (s), 933 (m), 915 (m), 891 (w), 864 (m), 825 (m), 798 (m), 771 (m), 764 (s), 741 (s), 692 (s), 660 (s). UV−vis (CH_2Cl_2, spiked with 5.7 mM pyridine): 909 nm (ε = 28 400 L mol^{-1} cm^{-1}), 677 (4940), 595 (sh, 3250), 486 (3780), 345 (sh, 6650), 298 (12 700). Anal. Calcd for $C_{57}H_{79}ClIrN_3O_2$: C, 64.23; H, 7.47; N, 3.94. Found: C, 64.23; H, 7.46; N, 3.88.

***cis*-(Diso)$_2$Ir(py)Cl.** In a 20 mL vial, $(Diso)_2IrCl$ (70.0 mg, 0.071 mmol) and pyridine (6.3 μL, 0.078 mmol) are dissolved in 3 mL of THF, and a stir bar is added. The vial is sealed, and the mixture is heated with stirring in a 70 °C oil bath for 30 min. After cooling to room temperature, the vial is opened to the air, and the solution is layered with methanol. The mixture is stored in a −20 °C freezer for a few days. The solid that forms is collected by suction filtration, washed with CH_3OH (2 × 5 mL), and dried in vacuo to afford 51.4 mg of *cis*-$(Diso)_2Ir(py)Cl$ (69%). ^1H NMR ($CDCl_3$, 23 °C): δ 8.86 (br, 1H, py), 7.85 (dd, 7.7, 1.2 Hz, 1H, NAr 3- or 5-H), 7.84 (dd, 7.7, 1.2 Hz, 1H, NAr 3- or 5-H), 7.65 (dd, 7.7, 1.2 Hz, 1H, NAr 3- or 5-H), 7.40 (br, 1H, py), 7.36 (tt, 7.4, 1.3 Hz, 1H, py 4-H), 7.24 (dd, 7.7, 1.2 Hz, 1H, NAr 3- or 5-H), 7.18 (t, 7.7 Hz, 1H, NAr 4-H), 7.09 (t, 7.7 Hz, 1H, NAr 4-H), 7.05 (br, 1H, py), 6.76 (br, 1H, py), 4.83 (s, 1H, iminoxolene 3- or 5-H), 4.76 (s, 1H, iminoxolene 3- or 5-H), 4.16 (s, 1H, iminoxolene 3- or 5-H), 3.68 (s, 1H, iminoxolene 3- or 5-H), 3.58 (sept, 6.5 Hz, 1H, $CHMe_2$), 3.25 (sept, 6.5 Hz, 1H, $CHMe_2$), 3.10 (sept, J = 6.5 Hz, 1H, $CHMe_2$), 2.11 (sept, 6.5 Hz, 1H, $CHMe_2$), 1.35 (d, 6.5 Hz, 3H, $CH(CH_3)Me$), 1.25 (s, 9H, ^{t}Bu), 1.23 (d, 6.5 Hz, 3H, $CH(CH_3)Me$), 1.22 (s, 9H, ^{t}Bu), 1.19 (s, 9H, ^{t}Bu), 1.17 (s, 9H, ^{t}Bu), 1.02 (d, 6.5 Hz, 3H, $CH(CH_3)Me$), 0.96 (d, 6.5 Hz, 3H, $CH(CH_3)Me$), 0.90 (d, 6.5 Hz, 3H, $CH(CH_3)Me$), 0.87 (d, 6.5 Hz, 3H, $CH(CH_3)Me$), 0.50 (d, 6.5 Hz, 3H, $CH(CH_3)Me$), −0.02 (d, 6.5 Hz, 3H, $CH(CH_3)Me$). $^{13}C\{^1H\}$ NMR ($CDCl_3$, 23 °C): δ 183.05 (br, *C*O), 181.77 (br, *C*O), 166.02 (br), 165.26 (br), 162.90 (br), 161.95 (br), 154.36 (br), 152.67 (br), 141.76 (br), 138.75 (br), 137.41, 136.99, 135.23, 133.84 (br), 133.30 (br), 129.47 (br), 128.44 (br), 127.91, 127.76, 126.73, 125.56, 125.42, 123.90, 123.68, 122.00 (br), 117.28, 115.90, 77.16, 36.57 ($C(CH_3)_3$), 36.19 ($C(CH_3)_3$), 33.68 ($C(CH_3)_3$), 33.37 ($C(CH_3)_3$), 32.91 ($C(CH_3)_3$), 32.85 ($C(CH_3)_3$), 28.20, 27.99, 27.75 ($C(CH_3)_3$), 27.56 ($C(CH_3)_3$), 27.17, 26.98, 27.01, 26.50, 25.78, 25.75, 25.68, 24.85, 23.66, 23.13. IR (cm^{-1}): 3057 (w), 2962 (m), 2951 (m), 2906 (m), 2867 (m), 1534 (m), 1518 (m), 1485 (m), 1457 (m), 1434 (m), 1381 (m), 1361 (m), 1326 (w), 1310 (m), 1296 (w), 1280 (w), 1246 (s), 1233 (s), 1216 (m), 1200 (s), 1162 (s), 1152 (m), 1114 (w), 1105 (m), 1072 (w), 1055 (w), 1024 (m), 995 (m), 951 (w), 934 (m), 914 (m), 865 (s), 825 (m), 800 (s), 771 (m), 760 (s), 741 (s), 717 (m), 692 (s). UV−vis (CH_2Cl_2): 1032 nm (ε = 12 600 L mol^{-1} cm^{-1}), 913 (sh, 9000), 712 (3690), 583 (3470), 497 (sh, 5000), 429 (7000), 347 (sh, 8400), 295 (18 100). CV: −1.40, −0.01, +0.60 V. Anal. Calcd for $C_{57}H_{79}ClIrN_3O_2$: C, 64.23; H, 7.47; N, 3.94. Found: C, 64.42; H, 7.54; N, 4.05.

***cis*-[(Diso)$_2$Ir(py)$_2$]Cl.** In the drybox, $(Diso)_2IrCl$ (87.3 mg, 0.088 mmol) is dissolved in 5 mL of $CHCl_3$ in a 20 mL vial, and a stir bar and pyridine (0.5 mL) are added. The vial is capped, and the reaction mixture is heated with stirring in a 52 °C oil bath for 2 d. The vial is opened to the air, filtered to remove a white solid, and the solvent stripped down on a rotary evaporator. The red solid is collected on a glass frit, washed with 3 × 10 mL of pentane, and air-dried for 30 min, yielding 38.9 mg of *cis*-$[(Diso)_2Ir(py)_2]Cl$ (39% yield). ^1H NMR ($CDCl_3$, 23 °C): δ 10.71 (d, 7.4 Hz, 2H, NAr 3- or 5-H), 10.09 (d, 7.6 Hz, 2H, NAr 3- or 5-H), 7.89 (sl br t, 7.4 Hz, 2H, py 4-H), 7.54 (br, 2H, py), 7.13 (br, 6H, py), 6.81 (t, 7.6 Hz, 2H, NAr 4-H), 4.22 (sl br sept, 5.1 Hz, 2H, $CHMe_2$), 2.52 (sl br sept, 5.1 Hz, 2H, $CHMe_2$), 1.97 (s, 18H, ^{t}Bu), 1.41 (d, 5.4 Hz, 6H, $CH(CH_3)Me$), 1.29 (s, 18H, ^{t}Bu), 1.11 (d, 5.3 Hz, 6H, $CH(CH_3)Me$), 0.67 (d, 5.6 Hz, 6H, $CH(CH_3)Me$), 0.24 (d, 5.5 Hz, 6H, $CH(CH_3)Me$), −2.56 (s, 2H, iminoxolene 3- or 5-H), −15.98 (s, 2H, iminoxolene 3- or 5-H). $^{13}C\{^1H\}$ NMR ($CDCl_3$, 23 °C): δ 154.43, 151.24, 140.92, 135.90, 131.86, 131.15, 126.82, 125.80, 113.79, 47.44, 42.86, 32.28, 27.98, 26.84, 24.86, 23.65, 23.61, 22.84, 18.84. IR (cm^{-1}): 3080 (w), 3071 (w), 2953 (m), 2925 (m), 2904 (m), 2865 (m), 1537 (w), 1521 (w), 1485 (w), 1463 (w), 1450 (m), 1428 (m), 1403 (w), 1393 (w), 1383 (w), 1362 (s), 1345 (w), 1310 (s), 1242 (s), 1213 (w), 1203 (m), 1182 (w), 1159 (s), 1115 (w), 1105 (m), 1094 (w), 1068 (w), 1052 (w), 1041 (w), 1026 (m), 995 (m), 952 (w), 931 (w), 910 (s), 869 (s), 824 (s), 806 (s), 768 (s), 764 (s), 743 (m), 719 (m), 708 (s), 695 (s), 682 (s), 668 (s), 664 (s). UV−vis (CH_2Cl_2): 1010 nm (9620 L mol^{-1} cm^{-1}), 865 (sh, 4700), 717 (sh, 3200), 560 (2920), 475 (6550), 410 (6710), 286 (21 000). CV: −1.63, −0.95, +0.29 V. Anal. Calcd for $C_{62}H_{84}ClIrN_4O_2$: C, 65.04; H, 7.39; N, 4.89. Found: C, 65.39; H, 7.17; N, 5.29.

X-ray Crystallography. Crystals of *trans*-$(Diso)_2Ir(py)Cl$ and *cis*-$(Diso)_2Ir(py)Cl{\cdot}PhCH_3$ were grown by diffusion of methanol into a solution of the complexes in THF and toluene, respectively. Crystals of *cis*-$(Diso)_2Ir(py)Cl{\cdot}CHCl_3$ were deposited from a solution of the complex. The mixed solvate *cis*-$[(Diso)_2Ir(py)_2]Cl{\cdot}4CHCl_3{\cdot}C_5H_{12}$ formed on diffusion of pentane into a chloroform solution of the complex. All crystals were placed in inert oil before being transferred to the cold N_2 stream of a Bruker Apex II diffractometer. The data were reduced, correcting for absorption, using the program SADABS. In the structure of *cis*-$[(Diso)_2Ir(py)_2]Cl{\cdot}4CHCl_3{\cdot}C_5H_{12}$, two chloroform molecules were found on difference Fourier maps and refined, but additional electron density resembling a pentane molecule could be observed but not satisfactorily refined. It was modeled using the SQUEEZE routine in PLATON,[23] which found 429 electrons per unit cell in a solvent-accessible volume of 2314 Å^3. This is consistent with one pentane per asymmetric unit. All nonhydrogen atoms were refined anisotropically, and hydrogen atoms were found on difference Fourier maps and refined isotropically. Calculations used SHELXTL (Bruker AXS),[24] with scattering factors and anomalous dispersion terms taken from the literature.[25]

Analysis of Singlet−Triplet Gaps by Variable-Temperature NMR Spectroscopy. NMR spectra were measured on a Bruker 400 MHz spectrometer. The samples were prepared in the drybox in either toluene-d_8 (*cis*-$(Diso)_2Ir(py)Cl$) or acetone-d_6 (*cis*-$[(Diso)_2Ir(py)_2]$-Cl) in Teflon-sealed screw-cap NMR tubes. Spectra were typically measured every 5 °C and referenced using the solvent residual signals (δ 2.08 for toluene-d_6 and 2.05 for acetone-d_6).

$$\delta_{obsd} = \delta_{dia,0\ °C} + \alpha(T - 273.15) + (63\,150)\frac{A}{T}(3 + e^{-\Delta E/0.001987T})^{-1} \quad (6)$$

The temperature-dependent behavior of the chemical shifts was modeled as described in the literature,[13] with ^1H NMR chemical shifts fit to eq 6, with δ in units of ppm, T in K, A in MHz, and ΔE in kcal mol^{-1}. In *cis*-$(Diso)_2Ir(py)Cl$, all aromatic resonances and the pyridine *para* resonance were modeled. For one doublet and one triplet resonance on the *N*-aryl ring, the corrections for the temperature dependence of the diamagnetic shift were not used (i.e., α was fixed at 0). In *cis*-$[(Diso)_2Ir(py)_2]Cl$, all resonances were modeled except for the pyridine meta signals. The iminoxolene peaks, one methine resonance, one *tert*-butyl resonance, and two aryl doublet resonances of the *N*-aryl rings were modeled with α fixed at 0. Unweighted nonlinear

https://doi.org/10.1021/acs.inorgchem.3c01717
Inorg. Chem. 2023, 62, 11718−11730

least-squares fitting was carried out using the Levenberg−Marquardt algorithm as implemented in the Solver routine of Microsoft Excel.[26] Global optima for these least-squares fits could be obtained in all cases. Uncertainties in the fitted parameters were estimated using standard methods.[27]

Measurement of Kinetics by Optical Spectroscopy. Optical spectra were acquired on an Agilent 8453 diode array spectrophotometer on samples in 1 cm cuvettes. For the addition of pyridine to $(Diso)_2IrCl$, solutions of pyridine in toluene at the desired concentration were prepared in the drybox. Approximately 2 mL of the solution was placed in a cuvette containing a small stir bar and sealed with a screw cap lined with a silicone septum. The cell was equilibrated at the desired temperature in a Unisoku CoolSpek cryostat, and the reaction was initiated by injecting 100 μL of a solution of $(Diso)_2IrCl$ in toluene into the cuvette while stirring. For the trans to cis isomerization reaction, solutions with the desired concentrations of both pyridine and $(Diso)_2IrCl$ were prepared in the glovebox and loaded into cuvettes sealed with Teflon needle valves. Reactions were initiated by placing the room-temperature cuvettes into a cell block preheated to 45.0 °C by an ethylene glycol/water mixture circulated through the cell block. The first 300 s of data was discarded as the temperature in the cuvettes equilibrated to the temperature of the cell block. Pseudo-first-order rate constants were obtained by fitting the absorbance at 900 nm (λ_{max} of *trans*-$(Diso)_2Ir(py)Cl$) or 705 nm (λ_{max} of $(Diso)_2IrCl$, used with very dilute solutions of pyridine) as a function of time to the expression $A = A_\infty + (A_0 - A_\infty)e^{-k_{obs}t}$ over at least four half-lives. Rate constants are reported as the average of at least three measurements.

Pyridine Exchange Kinetics by ^{1}H NMR Spectroscopy. In a typical experiment, approximately 10 mg of *cis*-$(Diso)_2Ir(py)Cl$ and 0.8 mg of dimethyl terephthalate standard were added to a screw-cap NMR tube in the air. The tube was then taken into the drybox, and 0.6 mL of toluene-d_8 and 10 equiv of pyridine-d_5 were added. The experiments were run in triplicate, with the second tube receiving 20 equiv of py-d_5 and the third tube receiving 30 equiv of py-d_5. The tubes were capped with a Teflon-lined screw cap, taken out of the drybox, and mixed thoroughly to ensure complete dissolution of the *cis*-$(Diso)_2Ir(py)Cl$ prior to taking an initial ^{1}H NMR spectrum. The tubes were then heated in a mineral oil bath at the desired temperature (81, 91, 100, 108.5, or 116 °C) and periodically removed to be assayed by ^{1}H NMR at room temperature as a function of the time spent in the oil bath. For each ^{1}H NMR spectrum, 4 scans were acquired with a 60 s relaxation delay. The peak for the 2,6-hydrogens of free pyridine at 8.51 ppm was integrated against dimethyl terephthalate's peak at 7.97 ppm, and the growth of this integral was fit to first-order kinetics as described above. Samples were monitored for at least three half-lives.

Computational Methods. Geometry optimizations were performed on simplified structures in which the *tert*-butyl groups were replaced by hydrogen and where the isopropyl groups were either present ("diso") or replaced with hydrogen ("ap"). Calculations used density functional theory (B3LYP, SDD basis set for Ir, 6-31G* basis set for all other atoms) as implemented in the Gaussian16 suite of programs.[28] The optimized geometries for stable species were confirmed as minima and transition states as first-order saddle points by calculation of vibrational frequencies. Plots of calculated Kohn−Sham orbitals were generated using GaussView (v. 6.0.16) with an isovalue of 0.04. Calculations on $(ap)_2IrCl$ have been reported previously.[6]

■ ASSOCIATED CONTENT

Supporting Information

The Supporting Information is available free of charge at https://pubs.acs.org/doi/10.1021/acs.inorgchem.3c01717.

NMR spectra, infrared spectra, UV−visible spectra, cyclic voltammograms, kinetics and thermodynamic data and plots, derivation of the rate law for trans to cis isomerization, calculated energies, MOS values, and Cartesian coordinates by DFT (PDF)

Accession Codes

CCDC 2261146−2261149 contain the supplementary crystallographic data for this paper. These data can be obtained free of charge via www.ccdc.cam.ac.uk/data_request/cif, or by emailing data_request@ccdc.cam.ac.uk, or by contacting The Cambridge Crystallographic Data Centre, 12 Union Road, Cambridge CB2 1EZ, UK; fax: +44 1223 336033.

■ AUTHOR INFORMATION

Corresponding Author

Seth N. Brown − *Department of Chemistry and Biochemistry, University of Notre Dame, Notre Dame, Indiana 46556-5670, United States*; orcid.org/0000-0001-8414-2396; Email: Seth.N.Brown.114@nd.edu

Authors

Thomas H. Do − *Department of Chemistry and Biochemistry, University of Notre Dame, Notre Dame, Indiana 46556-5670, United States*

David A. Haungs − *Department of Chemistry and Biochemistry, University of Notre Dame, Notre Dame, Indiana 46556-5670, United States*

William Y. Chin − *Department of Chemistry and Biochemistry, University of Notre Dame, Notre Dame, Indiana 46556-5670, United States*

Jack T. Jerit − *Department of Chemistry and Biochemistry, University of Notre Dame, Notre Dame, Indiana 46556-5670, United States*

Analena VanderZwaag − *Department of Chemistry and Biochemistry, University of Notre Dame, Notre Dame, Indiana 46556-5670, United States*

Complete contact information is available at: https://pubs.acs.org/10.1021/acs.inorgchem.3c01717

Notes

The authors declare no competing financial interest.

■ ACKNOWLEDGMENTS

This work was supported by the US National Science Foundation (CHE-1955933). We thank Dr. Allen G. Oliver for his assistance with X-ray crystallography and Prof. Emily Tsui for the use of the UV−vis cryostat. We thank Claire Nkwo and Kang-Young Kim for their preliminary investigations of the trans to cis isomerization kinetics. T.H.D. acknowledges support via an Arthur J. Schmitt Fellowship, and W.Y.C. and J.T.J. acknowledge support from the Notre Dame College of Science (Summer Undergraduate Research Fellowships).

■ REFERENCES

(1) Tobe, M. L. Base Hydrolysis of Octahedral Complexes. *Acc. Chem. Res.* **1970**, *3*, 377−385.

(2) Pearson, R. G.; Basolo, F. Mechanism of Substitution Reactions of Complex Ions. X. π-Bonding in Dissociation Reactions of Octahedral Complexes. *J. Am. Chem. Soc.* **1956**, *78*, 4878−4883.

(3) Eisenberg, R.; Gray, H. B. Noninnocence in Metal Complexes: A Dithiolene Dawn. *Inorg. Chem.* **2011**, *50*, 9741−9751.

(4) Marshall-Roth, T.; Brown, S. N. Redox activity and π bonding in a tripodal seven-coordinate molybdenum(VI) tris(amidophenolate). *Dalton Trans.* **2015**, *44*, 677−685.

(5) Gianino, J.; Brown, S. N. Highly covalent metal−ligand π bonding in chelated bis- and tris(iminoxolene) complexes of osmium and ruthenium. *Dalton Trans.* **2020**, *49*, 7015−7027.

(6) Do, T. H.; Brown, S. N. Mono- and Bis(iminoxolene)iridium Complexes: Synthesis and Covalency in π Bonding. *Inorg. Chem.* **2022**, *61*, 5547−5562.
(7) Haungs, D. A.; Brown, S. N. Slicing the π in Three Unequal Pieces: Iridium Complexes with Alkyne, Iminoxolene, and Dioxolene Ligands. *Organometallics* **2022**, *41*, 3612−3626.
(8) (a) Hückstädt, H.; Homborg, H. Synthesis of Bis[pyridine-phthalocyaninato(1,5-)iridium(II)] Iodide and Pyridine-iodo-Phthalocyaninato(2-)iridium(III)-Pyridine by Successive Oxidation of Bis[pyridine-phthalocyaninato(2-)iridium(II)]. *Z. Naturforsch., B: J. Chem. Sci.* **1997**, *52*, 728−734. (b) Albertí, F. M.; Fiol, J. J.; García-Raso, A.; Torres, M.; Terrón, A.; Barceló-Oliver, M.; Prieto, M. J.; Moreno, V.; Molins, E. Ruthenium(III) and iridium(III) complexes with nicotine. *Polyhedron* **2010**, *29*, 34−41.
(9) (a) Edwards, N. S. A.; Gillard, R. D.; Hursthouse, M. B.; Lieberman, H. F.; Abdul Malik, K. M. Equilibria in Complexes of *N*-Heterocyclic Compounds—LI. Synergic Solubility and X-Ray Crystal Structure Analysis of *mer*-Chloro-Oxalato-Tris-Pyridine-Iridium(III), $[IrCl(py)_3(C_2O_4)]$. *Polyhedron* **1993**, *12*, 2925−2928. (b) Tenn, W. J.; Young, K. J. H.; Bhalla, G.; Oxgaard, J.; Goddard, W. A.; Periana, R. A. CH Activation with an O-Donor Iridium−Methoxo Complex. *J. Am. Chem. Soc.* **2005**, *127*, 14172−14173. (c) Tenn, W. J.; Young, K. J. H.; Oxgaard, J.; Nielsen, R. J.; Goddard, W. A.; Periana, R. A. Heterolytic CH Activation and Catalysis by an O-Donor Iridium−Hydroxo Complex. *Organometallics* **2006**, *25*, 5173−5175.
(10) Brown, S. N. Metrical Oxidation States of 2-Amidophenoxide and Catecholate Ligands: Structural Signatures of Metal−Ligand π Bonding in Potentially Noninnocent Ligands. *Inorg. Chem.* **2012**, *51*, 1251−1260.
(11) Erickson, A. N.; Gianino, J.; Markovitz, S. J.; Brown, S. N. Amphiphilicity in Oxygen Atom Transfer Reactions of Oxobis-(iminoxolene)osmium Complexes. *Inorg. Chem.* **2021**, *60*, 4004−4014.
(12) Hübner, R.; Sarkar, B.; Fiedler, J.; Záliš, S.; Kaim, W. Metal(IV) Complexes $[M(L_{N,O,S})_2]^n$ (M = Ru, Os) of a Redox-Active *o*-Amidophenolate Ligand $(L_{N,O,S})^{2-}$ with Coordinating Thioether Appendix. *Eur. J. Inorg. Chem.* **2012**, *2012*, 3569−3576.
(13) Conner, K. M.; Perugini, A. L.; Malabute, M.; Brown, S. N. Group 10 Bis(iminosemiquinone) Complexes: Measurement of Singlet−Triplet Gaps and Analysis of the Effects of Metal and Geometry on Electronic Structure. *Inorg. Chem.* **2018**, *57*, 3272−3286.
(14) Marshall-Roth, T.; Yao, K.; Parkhill, J. A.; Brown, S. N. On the border between localization and delocalization: tris(iminoxolene)-titanium(IV). *Dalton Trans.* **2019**, *48*, 1427−1435.
(15) (a) Cotton, F. A.; Eglin, J. L.; Hong, B.; James, C. A. Singlet−Triplet Separations Measured by $^{31}P\{^1H\}$ NMR: Applications to Quadruply Bonded Dimolybdenum and Ditungsten Complexes. *Inorg. Chem.* **1993**, *32*, 2104−2106. (b) Cotton, F. A.; Su, J.; Sun, Z. S.; Chen, H. Preparation and Structural Characterization of $Mo_2Cl_4(OAc)_2(PR_3)_2$ Compounds (R = Me, Et) and a Comparative Study of the Singlet−Triplet Separation for $Mo_2Cl_4(OAc)_2(PEt_3)_2$ with That for $Mo_2Cl_6(dppm)_2$. *Inorg. Chem.* **1993**, *32*, 4871−4875. (c) Le Guennic, B.; Floyd, T.; Galan, B. R.; Autschbach, J.; Keister, J. B. Paramagnetic Effects on the NMR Spectra of "Diamagnetic" Ruthenium (bis-phosphine)(bis-semiquinone) Complexes. *Inorg. Chem.* **2009**, *48*, 5504−5511. (d) Pfirrmann, S.; Limberg, C.; Herwig, C.; Knispel, C.; Braun, B.; Bill, E.; Stösser, R. A Reduced β-Diketiminato-Ligated Ni_3H_4 Unit Catalyzing H/D Exchange. *J. Am. Chem. Soc.* **2010**, *132*, 13684−13691.
(16) Shekar, S.; Brown, S. N. Mixed amidophenolate−catecholates of molybdenum(VI). *Dalton Trans.* **2014**, *43*, 3601−3611.
(17) Erickson, A. N.; Brown, S. N. Molybdenum(VI) tris-(amidophenoxide) complexes. *Dalton Trans.* **2018**, *47*, 15583−15595.
(18) McKay, H. A. C. Kinetics of Exchange Reactions. *Nature* **1938**, *142*, 997−998.
(19) Henderson, R. A.; Tobe, M. L. Effect of Steric Constraints on the Rates of Base Hydrolysis of Cobalt(III) Complexes. *Inorg. Chem.* **1977**, *16*, 2576−2583.
(20) Abakumov, G. A.; Druzhkov, N. O.; Kurskii, Y. A.; Shavyrin, A. S. NMR study of products of thermal transformation of substituted *N*-aryl-*o*-quinoneimines. *Russ. Chem. Bull.* **2003**, *52*, 712−717.
(21) Connelly, N. G.; Geiger, W. E. Chemical Redox Agents for Organometallic Chemistry. *Chem. Rev.* **1996**, *96*, 877−910.
(22) Lionetti, D.; Medvecz, A. J.; Ugrinova, V.; Quiroz-Guzman, M.; Noll, B. C.; Brown, S. N. Redox-Active Tripodal Aminetris(aryloxide) Complexes of Titanium(IV). *Inorg. Chem.* **2010**, *49*, 4687−4697.
(23) van der Sluis, P.; Spek, A. L. BYPASS: an Effective Method for the Refinement of Crystal Structures Containing Disordered Solvent Regions. *Acta Crystallogr., Sect. A: Found. Crystallogr.* **1990**, *46*, 194−201.
(24) Sheldrick, G. M. A short history of SHELX. *Acta Crystallogr., Sect. A: Found. Crystallogr.* **2007**, *64*, 112−122.
(25) Wilson, A. J. C.; Geist, V. *Mathematical, Physical and Chemical Tables*; International Tables for Crystallography; Kluwer Academic Publishers: Dordrecht/Boston/London, 1992; Volume C.
(26) Harris, D. C. Nonlinear Least-Squares Curve Fitting with Microsoft Excel Solver. *J. Chem. Educ.* **1998**, *75*, 119−121.
(27) de Levie, R. Estimating Parameter Precision in Nonlinear Least Squares with Excel's Solver. *J. Chem. Educ.* **1999**, *76*, 1594−1598.
(28) Frisch, M. J.; Trucks, G. W.; Schlegel, H. B.; Scuseria, G. E.; Robb, M. A.; Cheeseman, J. R.; Scalmani, G.; Barone, V.; Petersson, G. A.; Nakatsuji, H.; Li, X.; Caricato, M.; Marenich, A. V.; Bloino, J.; Janesko, B. G.; Gomperts, R.; Mennucci, B.; Hratchian, H. P.; Ortiz, J. V.; Izmaylov, A. F.; Sonnenberg, J. L.; Williams-Young, D.; Ding, F.; Lipparini, F.; Egidi, F.; Goings, J.; Peng, B.; Petrone, A.; Henderson, T.; Ranasinghe, D.; Zakrzewski, V. G.; Gao, J.; Rega, N.; Zheng, G.; Liang, W.; Hada, M.; Ehara, M.; Toyota, K.; Fukuda, R.; Hasegawa, J.; Ishida, M.; Nakajima, T.; Honda, Y.; Kitao, O.; Nakai, H.; Vreven, T.; Throssell, K.; Montgomery, J. A., Jr.; Peralta, J. E.; Ogliaro, F.; Bearpark, M. J.; Heyd, J. J.; Brothers, E. N.; Kudin, K. N.; Staroverov, V. N.; Keith, T. A.; Kobayashi, R.; Normand, J.; Raghavachari, K.; Rendell, A. P.; Burant, J. C.; Iyengar, S. S.; Tomasi, J.; Cossi, M.; Millam, J. M.; Klene, M.; Adamo, C.; Cammi, R.; Ochterski, J. W.; Martin, R. L.; Morokuma, K.; Farkas, O.; Foresman, J. B.; Fox, D. J. *Gaussian 16*, Revision C.01; Gaussian, Inc.: Wallingford CT, 2016.

https://doi.org/10.1021/acs.inorgchem.3c01717
Inorg. Chem. 2023, 62, 11718−11730